EURASIP Journal on Applied Signal Processing 2005:14, 2207–2214

Selective Synthetic Aperture Radar and Panchromatic Image Fusion by Using the à Trous Wavelet Decomposition

Youcef Chibani

Laboratoire de Traitement du Signal, Faculté d'Electronique et d'Informatique, Université des Sciences et de la Technologie Houari Boumediene, BP 32, El-Alia, Bab-Ezzouar, 16111 Algiers, Algeria
Email: ychibani@usthb.dz

Received 24 December 2003; Revised 9 January 2005

Synthetic aperture radar (SAR) imaging sensor presents an important advantage for the earth change observation independently of weather conditions. However, the SAR image provides an incomplete information (as roads) of the observed scene leading thus to an ambiguous interpretation. In order to compensate the lack of features, the high spatial resolution panchromatic (P) image is often used as a complementary data for improving the quality of the SAR image. The concept is based on the extraction of features (details) from the P image in order to incorporate into the SAR image. Therefore, we propose an approach based on the use of the *à trous* wavelet decomposition (ATWD) for extracting features from the P image. Experimental results show that the SAR-*P* composite image allows a better detection of lines, edges, and field boundaries.

Keywords and phrases: remote sensing, SAR and panchromatic images, image fusion, highpass filtering, à trous wavelet decomposition.

1. INTRODUCTION

In remote sensing, the synthetic aperture radar (SAR) imaging sensor presents an important advantage for the earth change observation independently of weather conditions. Its sensitivity to the geometry of targets allows providing an image that essentially contains information on the surface roughness, object shape, orientation, as well as the moisture content [1, 2]. A second advantage is the increase of the values for urban features because of the corner reflector effect. However, the recognition of some features as roads or fields boundaries is more difficult in some areas of the scene; the degree of difficulty depends on their structure, extent, and orientation [3]. For example, line features that run parallel to the flight path, that is, perpendicular to the SAR beam, are clearly visible. Others that are running across track are not imaged at all. Also, the only use of the SAR image leads to a difficult interpretation of the scene [1].

In order to improve the quality of the SAR image, the panchromatic (P) image is often used as a complementary data [4] since it is captured in the visible band and characterized by high spatial information content well suited to intermediate scale mapping applications and urban analysis. The concept is based on the extraction of features (details) from the P image, by means of an appropriate algorithm, in order to incorporate into the SAR image. Usually, the highpass filtering (HPF) is the method used for extracting features [4]. However, the arbitrary choice of the filter coefficients (size and shape) complicates its use. An alternative approach is the use of the wavelet transform as a method for characterizing features of the image.

Usually, the wavelet transform is described as a multiresolution decomposition [5]. It is based on the orthogonal decomposition of the image onto a wavelet basis in order to avoid a redundancy of information in the pyramid at each level of resolution. An alternative approach, based on the nonorthogonal decomposition of the image, has been developed for fusing multisensor images [6, 7]. Its advantage lies in the analysis pixel by pixel, without decimation, for the characterization of features, and corresponds to an overcomplete representation. Unlike the orthogonal wavelet decomposition, the nonorthogonal wavelet decomposition may be redundant. It is accomplished by using the "*à trous*" algorithm [8, 9].

Therefore, we propose a feature extraction method from the P image based on the use of the "à trous" wavelet decomposition. The features are injected into the SAR image by selecting the only important wavelet coefficients in order to avoid the disturbance of the information content.

The next sections of this paper are organized as follows. In Section 2, we describe the methodology adopted for improving the SAR image. Section 3 presents the experimental results realized on SPOT and RADARSAT satellite images. Finally, the conclusion is given in Section 4.

2. METHODOLOGY

2.1. Highpass filtering method

Highpass filtering (HPF) method is usually used for extracting features (or details) contained in an image [10]. It has been initially developed for improving the spatial resolution of multispectral images. Its concept is based on the application of a highpass filter on the image in order to isolate information of high spatial frequencies. The resulting image is then added, pixel by pixel, to the multispectral image of lower spatial resolution. Formally, each detail can be extracted from the panchromatic image by means of the following equation:

$$\Delta P(k,l) = P(k,l) - \bar{P}(k,l), \tag{1}$$

$\Delta P(k,l)$ denotes the local detail, whereas $P(k,l)$ is the pixel intensity and $\bar{P}(k,l)$ is its filtered value, which corresponds to the lowpass filtering operation such that

$$\bar{P}(k,l) = \frac{1}{\#W} \sum_m \sum_n c(m,n) P(k+m, l+n), \tag{2}$$

$c(m,n)$ are coefficients of the lowpass filter and $\#W$ is the number of filter coefficients.

The simplicity of this method allows envisaging its use for improving the quality of the SAR image. For this, each detail extracted from the P image will be added to the SAR image, termed $R(k,l)$, to produce an improved SAR-P fused image, termed $\hat{R}(k,l)$. This translates to the following equation:

$$\hat{R}(k,l) = R(k,l) + \Delta P(k,l). \tag{3}$$

The use of the HPF method is complicated by the arbitrary choice of the filter coefficients (shape and size) for extracting features. Generally, the coefficients of the lowpass filter are simply chosen identical to one. Thus, the filtered value corresponds to the computation of the local mean where pixels contribute of equivalent manner. However, the filtered value does not really reflect the local characteristics of the image since it contains complex features as edges.

It becomes useful to modelize features by means of an efficient mathematical tool that allows taking into account the local characteristics of the image. Hence, the wavelet decomposition may be an appropriate solution since the wavelet coefficient amplitude allows informing on the importance of the feature contained into the image. In our approach, we use the "à trous" wavelet decomposition (ATWD) for extracting the image features. For a more comprehensive presentation of the integration method, we briefly review the main properties of the ATWD and its implementation by means of filters.

2.2. À trous wavelet decomposition

Usually, the wavelet decomposition is described as an orthogonal multiresolution representation [5, 11] and has been extensively used for fusing multisensor images [12, 13, 14]. More recently, an evaluation study has proved that the orthogonalwavelet decomposition is not appropriate for image fusion since it has some limited performances [7]. An alternative approach has been proposed using the "*à trous*" wavelet decomposition (ATWD), which presents the interesting properties as [15] follows:

(i) the algorithm produces a single wavelet coefficient plane at each level of decomposition,
(ii) the wavelet coefficients are computed for each location allowing a better detection of a dominant feature,
(iii) the dominant feature can be followed from scale to scale,
(iv) the algorithm is easily implemented.

The ATWD of a discrete signal $s(k)$ allows the separation of low-frequency information (approximation) from high-frequency information (wavelet coefficients). Such a separation requires the use of a lowpass filter $h(n)$, associated with the scale function $\varphi(x)$, to obtain several undecimated successive approximations of a signal through scales:

$$s_j(k) = \sum_n h(n) s_{j-1}(k + n2^{j-1}), \quad j = 1, \ldots, N, \tag{4}$$

$s_0(k)$ corresponds to the original discrete signal $s(k)$; j and N are the scale index and the number of scales, respectively. The wavelet coefficients are extracted by using the highpass filter $g(n)$, associated with the wavelet function $\psi(x)$, through the following filtering operation:

$$w_j(k) = \sum_n g(n) s_{j-1}(k + n2^{j-1}). \tag{5}$$

The exact reconstruction of the signal $s(k)$ is performed by introducing two dual filters $\bar{h}(n)$ and $\bar{g}(n)$ that should satisfy the quadrature mirror filter (QMF) condition [9]:

$$\bar{h}(n)^* h(n) + \bar{g}(n)^* g(n) = \delta(n), \tag{6}$$

where $\delta(n)$ is the impulse function and $*$ denotes the convolution operator.

Since (6) offers more degrees of freedom, a simple choice consists in considering $\bar{h}(n)$ and $\bar{g}(n)$ filters as equal to the impulse function ($\bar{h}(n) = \bar{g}(n) = \delta(n)$). Therefore, $g(n)$ is deduced from (6) as

$$g(n) = \delta(n) - h(n). \tag{7}$$

By replacing (7) in (5), the wavelet coefficients are obtained by a straightforward difference between two successive approximations as follows:

$$w_j(k) = s_{j-1}(k) - s_j(k). \tag{8}$$

The reconstruction of the original signal $s(k)$ is simply obtained by adding the last smoothed signal $s_N(k)$ with the set of the wavelet coefficients, let

$$s(k) = s_N(k) + \sum_{j=1}^{N} w_j(k). \tag{9}$$

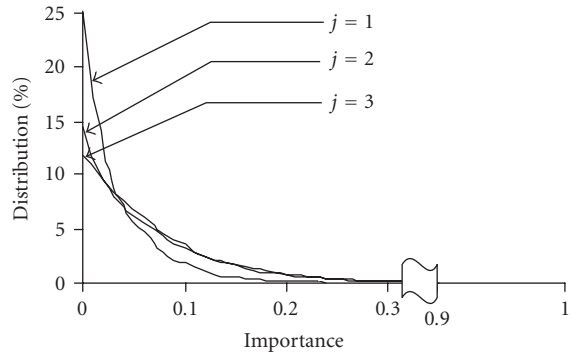

Figure 1: Distribution of the importance values computed for each scale ($j = 1, 2, 3$).

Figure 2: Panchromatic image.

It is interesting to note that the HPF method is a particular case of the ATWD when all filter coefficients $h(n)$ take the same values at the scale $N = 1$. Therefore, the main advantage of the ATWD lies in the appropriate choice of the filter coefficients where values are directly tied to the properties of the scale function. Generally, the filter coefficients are deduced from the function having a B_3 cubic spline scale profile [15].

The ATWD for an image is accomplished by a separable filtering following rows and columns, respectively. Specifically, a single wavelet plane is produced at each scale by subtraction of two successive approximations without decimation. Thus, wavelet and approximation planes have the same dimensions as the original image. As a consequence, the ATWD produces a redundancy of features from scale to another when those are dominant.

2.3. Integration scheme

The methodology adopted for improving the SAR image is accomplished in two steps:

(i) feature extraction from the panchromatic (P) image by using the ATWD;
(ii) incorporation of features into the SAR image by a selective addition procedure.

More precisely, the P image is decomposed by the ATWD in several scales:

$$P(k,l) = P_N(k,l) + \sum_{j=1}^{N} w_j^P(k,l), \tag{10}$$

where $P_N(k,l)$ corresponds to the last approximation plane and $w_j^P(k,l)$ is the wavelet coefficient computed for each location (k,l) and at each scale j. Thus, the wavelet coefficients are added, pixel by pixel and scale by scale, to the SAR image in order to produce the SAR-P composite image:

$$\hat{R}(k,l) = R(k,l) + \sum_{j=1}^{N} w_j^P(k,l). \tag{11}$$

In this equation, $R(k,l)$ can be interpreted as the last approximation plane of the improved SAR image $\hat{R}(k,l)$.

The full integration of P features into the SAR image can mask and disturb small features as the surface roughness, which can be important for the interpretation of the scene. Thus, the amount of features incorporated into the SAR image can be controlled by selecting the wavelet coefficients by means of the following equation:

$$\hat{R}(k,l) = R(k,l) + \sum_{j=1}^{N} \alpha_j(k,l) w_j^P(k,l), \tag{12}$$

where $\alpha_j(k,l)$ is a binary factor which can take the two following values:

$$\alpha_j(k,l) = \begin{cases} 1 & \text{if } w_j^P(k,l) \text{ is selected,} \\ 0 & \text{elsewhere.} \end{cases} \tag{13}$$

The selection of a significant wavelet coefficient depends on its amplitude value. Thus, a wavelet coefficient is considered important when it acquires high amplitude (with negative or positive sign). Hence, the value of a coefficient for a particular location, and any scale, can be understood as a measure of the feature importance. Therefore, we define the importance of a wavelet coefficient through the following measure:

$$g_j^P(k,l) = \frac{|\, w_j^P(k,l) \,|}{\mathrm{Max}_{k,l} \{\, |\, w_j^P(k,l) \,| \,\}}, \tag{14}$$

where $g_j^P(k,l)$ is the importance value and lies in the range $[0, 1]$. $\mathrm{Max}_{k,l}\{|w_j^P(k,l)|\}$ denotes the absolute maximal amplitude of the wavelet coefficient determined at the scale j. Figure 1 shows the distribution of the importance values computed from the P image (Figure 2). We can note that this distribution is similar to the generalized Gaussian.

It is interesting to consider three particular cases through the importance values:

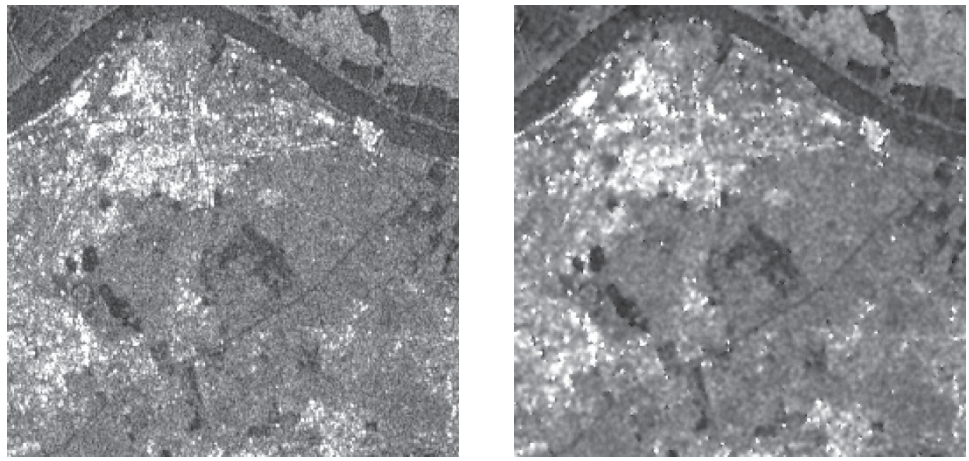

(a) (b)

Figure 3: SAR images: (a) unfiltered SAR image; (b) filtered SAR image.

(i) when the importance value is near zero, $g_j^P(k,l) \approx 0$, the distribution informs that the P image contains many flat areas;

(ii) when the importance value is near one, $g_j^P(k,l) \approx 1$, the distribution informs on the presence of a point object;

(iii) the intermediate values, $g_j^P(k,l) \in]0,1[$, correspond to features having medium amplitudes as textures and transition lines.

From these considerations, a wavelet coefficient is selected through its importance value by choosing a threshold noted τ_j depending on the scale index j:

$$\alpha_j(k,l) = \begin{cases} 1 & \text{if } g_j^P(k,l) \geq \tau_j, \\ 0 & \text{elsewhere.} \end{cases} \tag{15}$$

Note that the sign of the wavelet coefficient should be preserved in order to generate the local variations between pixels into the SAR image. Hence, each feature $w_j^P(k,l)$ having an importance value $g_j^P(k,l)$ between τ_j and 1 is incorporated into the SAR image. The adjustment of the threshold from one (point object) to zero (flat area) allows incorporating gradually the features into the SAR image.

3. EXPERIMENTAL RESULTS

3.1. Image preparation

Images used for our experimentation are captured from RADARSAT and SPOT satellites, covering a region of Vietnam and more precisely the Haïphong Bay located at 107° E and 21° N. The region is a land plane and comprises a village with small houses, a peach port, and agricultural fields. Our investigation is carried out on the basis of the following data:

(i) SPOT-P data, acquired vertically on 21 October 1992 with a 10 m spatial resolution;

(ii) RADARSAT-SAR data, acquired on 15 December 1996 with a 12.5 m pixel size and an incidence angle of 23°.

Two particular preprocessing should be applied to SAR and P images before the application of an integration method [4]. In the case of the SAR image, two elementary operations are used: speckle reduction and conversion from 16 bits to 8 bits. The speckle reduction allows avoiding eventual ambiguities for the interpretation of the scene. Various sophisticated methods have been developed for reducing the speckle. In this experimentation, the SAR image coded in 16 bits is filtered by using the standard Lopes filter with a window of 5×5 [16] since it allows retaining texture information, linear features, and point target responses. The conversion of the SAR image allows ensuring a correct combination with the P image (delivered in 8 bits). Therefore, the filtered SAR image is converted from 16 bits to 8 bits by matching the histogram of both P and SAR images. More precisely, after computing the histogram of both P and SAR images, the histogram of the SAR image is modified according to the histogram of the P image. Obviously,other conversion and recent filtered methods can be used according to applications [4].

The second preprocessing is the coregistration procedure. As the considered region is a flat terrain, a polynomial method is used to register geometrically the SAR and P images. Therefore, a number of well-distributed and accurately ground control points are selected in both images in order to compute the polynomial coefficients. P image is considered as the reference since it has superior spatial resolution and provides more details compared to the SAR image. The coregistration error is less than 0.7 pixel. The SAR image is resampled to 10 m according to the spatial resolution of the P image. Figures 2, 3a, and 3b show, respectively, the P, unfiltered and filtered SAR images corresponding to a 512-by-512 pixel area.

3.2. SAR-P composite image presentation

To show the utility of the ATWD for improving the SAR image, we compare it with the HPF method. The ATWD is

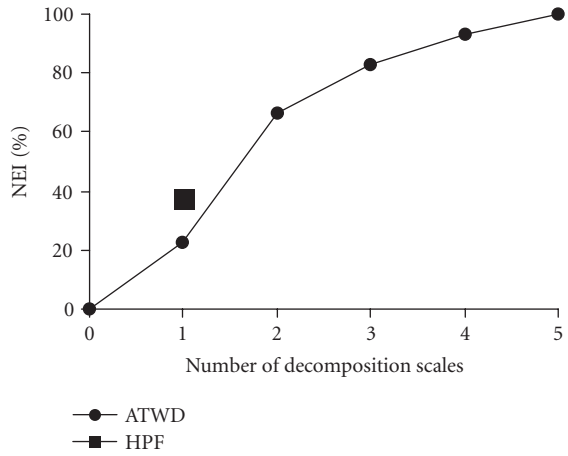

Figure 4: Normalized entropy information versus number of decomposition scales computed for SAR-*P* composite image.

performed on the P image by using a mask of 5×5 [17]. The composite image is named SAR-*P*, which corresponds to the integration of *P* features into the SAR image. For an objective evaluation, we also use the same size for the computation of the mean in the HPF method. Hence, the performance of each method is evaluated by considering two points: the required number of decomposition scales and the adjustment of the threshold.

The required number of decomposition scales constitutes the first step before the adjustment of the threshold. Hence, we consider an objective measure based on the normalized entropy information (NEI) that allows evaluating precisely the amount of features incorporated into an image [6]. More precisely, the NEI (expressed in %) provides a larger amount of features incorporated into the SAR image than that initially contained into the SAR image. Thus, the initial SAR image has an NEI = 0%, while NEI = 100% corresponds to the maximal integration of *P* features into the SAR image.

Figure 4 presents the NEI computed from the SAR-*P* composite image produced by the ATWD. Five scales of decomposition are considered by taking the threshold zero at each scale ($\tau_j = 0$). For $N = 0$, any feature is incorporated into the SAR image (NEI = 0%); whereas for $N = 5$, all features contained between scales 1 to 5 are incorporated into the SAR image (NEI = 100%). NEI is also evaluated on the SAR-*P* composite image produced from the HPF method.

For $N = 1$, the HPF method provides a greater NEI (37%) compared to ATWD (22%). By adding features contained between scales 1 and 5, we can note that the NEI increases significantly between scales 2 (65%) and 3 (82%). This denotes that the features are essentially presented between scales 1 and 3. Hence, three scales of decomposition are sufficient for incorporating the important features coming from the P image into the SAR image.

Visually speaking, for a threshold $\tau_j = 0$, SAR-*P* composite images produced from the HPF method (Figure 5a) and the ATWD with $N = 1$ (Figure 5b) are comparable in terms of incorporated features. Many important features as lines and edges do not significantly appear more specifically with the ATWD. For $N = 3$ (Figure 5c), important features coming from the P image are incorporated into the SAR image. Linear and transition features are well represented and allow pointing out the road infrastructures and field boundaries. However, an important disturbance can be observed especially in flat areas where information corresponding to the surface roughness provided by the SAR image is discarded which can be important for the interpretation of the scene. Hence, an adjustment of the threshold is required for controlling efficiently the amount of features incorporated into the SAR image.

Basically, the threshold can be adjusted at each scale. With $N = 3$, three thresholds should be adjusted in order to find the best values. In this experimentation, we use an alternative way, which consists in adjusting the threshold with the same value at each scale. Such a way allows incorporating in a similar manner all features having an importance value comprised between τ_j and 1. Hence, an only adjustment of the threshold is required for all scales. Figure 6 shows the NEI obtained by varying the threshold from 0.01 to 1 with a logarithmic step. The trend of the curve indicates an important increase of features for a threshold comprised between 0.30 (NEI = 13%) and 0.10 (NEI = 75%).

Figure 5d shows the SAR-*P* composite image produced from the ATWD with a threshold $\tau_j = 0.15$. We can note that the linear and transition features are mainly incorporated into the SAR image without a considerable disturbance of the surface roughness. The threshold can thus be considered as an adjustable parameter that allows selecting easily the important features.

3.3. Discussion

Except the presence of the speckle noise, which can be reduced by using various methods, the lack of some features is the main difficulty for the correct interpretation of the SAR

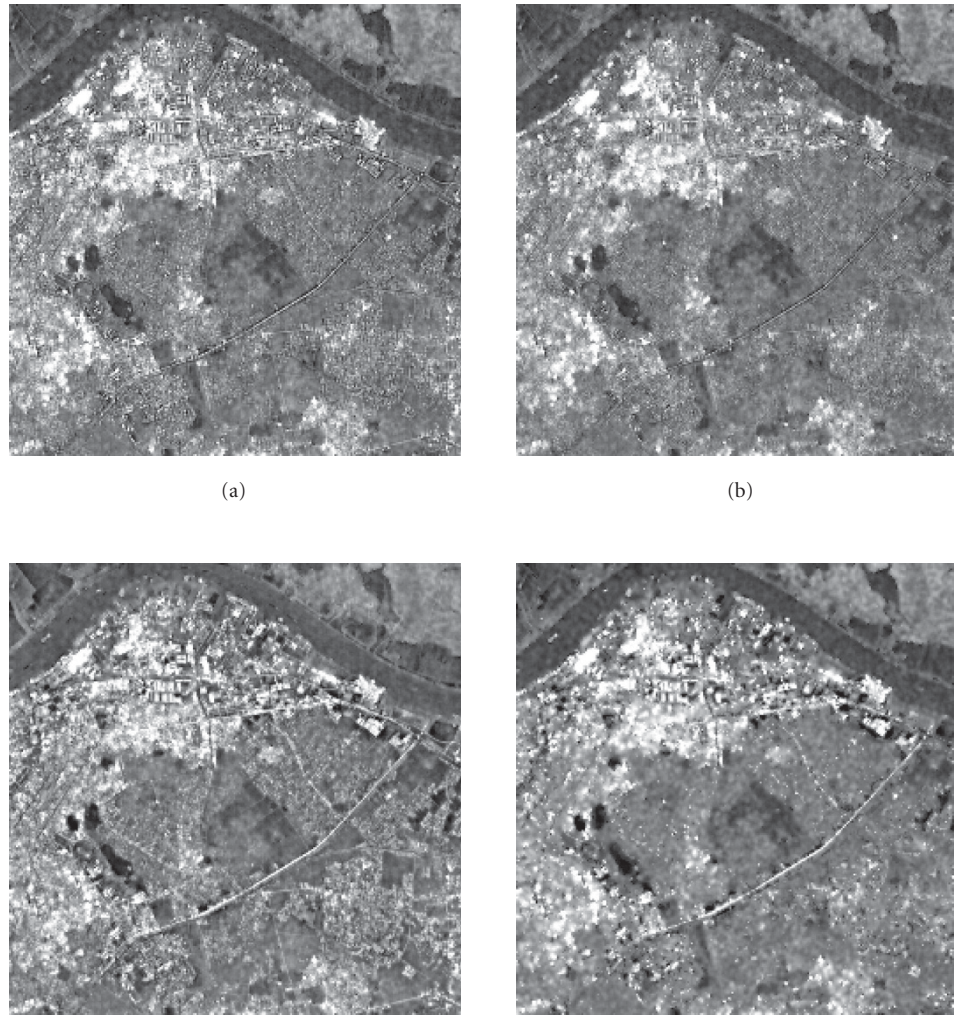

(a) (b)

(c) (d)

Figure 5: SAR-*P* composite image obtained by using HPF method and ATWD with several scales and thresholds: (a) HPF; (b) ATWD: $N = 1$, $\tau_j = 0$; (c) ATWD: $N = 3$, $\tau_j = 0$; (d) ATWD: $N = 3$, $\tau_j = 0.15$.

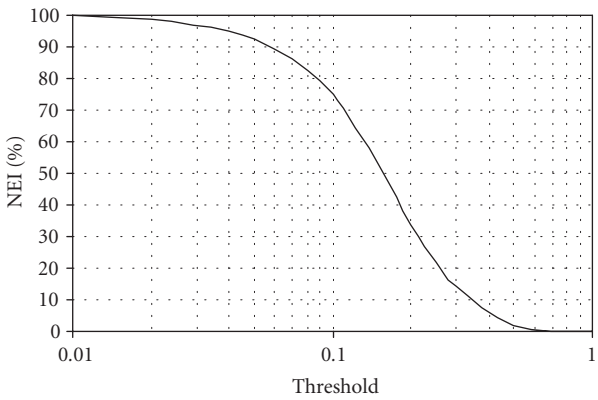

Figure 6: Normalized entropy information versus threshold computed for the SAR-*P* composite image.

image. To enhance its quality, the P image is used as a complementary data. Hence, the HPF method is usually used for extracting features from the P image in order to incorporate into the SAR image. However, the SAR-*P* composite image produced by the HPF method does not allow an easy interpretation of the scene since features incorporated into the SAR image are not significantly enhanced. This limitation arises from the arbitrary choice of filter coefficients whose values do not correctly reflect the local variations of the image. This limitation can be overcome by using the ATWD that allows an efficient characterization of features contained in the P image.

Although the ATWD requires more calculations and memories than the HPF method, the visual appreciation shows that the ATWD produces an SAR-*P* composite image better than the HPF method. As the SAR image already

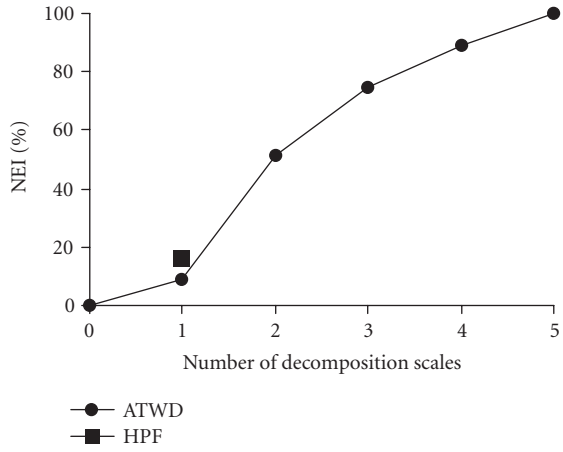

Figure 7: Normalized entropy information versus number of decomposition scales computed for the P-SAR composite image.

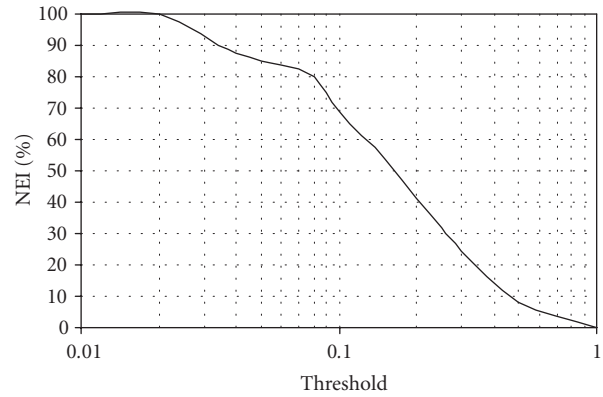

Figure 8: Normalized entropy information versus threshold computed for the P-SAR composite image.

provides information on the roughness and point target responses, SAR-*P* composite images point out the contribution of high spatial frequencies for the detection of roads and parcel arrangements. The P image has an effect on the discrimination of lines and edges in the SAR image.

The choice of features to be incorporated constitutes an interesting aspect to ensure an efficient improvement of the SAR image. An adjustable threshold allows thus a selection of features according the importance value of the wavelet coefficient. Hence, the appropriate choice of the threshold constitutes a flexible parameter for the user since it has the possibility to control the amount of features to be incorporated into the SAR image.

The proposed method can also be used for incorporating the SAR features into the P image. In this case, the composite image is named P-SAR. Since the SAR imaging sensor is sensitive to the geometry of targets, the P-SAR composite image allows pointing out mainly the point targets and the surface roughness into the P image.

Figure 7 presents the NEI computed from the P-SAR composite image produced by the ATWD. Five scales of decomposition are considered by taking the threshold zero at each scale ($\tau_j = 0$). As we can see, three scales of decomposition are sufficient (NEI = 75%) for incorporating the important features coming from the SAR image into the P image. Figure 8 shows the NEI obtained by varying the threshold from 0.01 to 1 with a logarithmic step. The trend of the curve indicates an important increase of features for a threshold comprised between 0.50 (NEI = 10%) and 0.08 (NEI = 81%).

Figure 9a shows the P-SAR composite image (corresponding to the integration of *P* features into the SAR image) produced from the ATWD with a threshold $\tau_j = 0$. We can note that the SAR features corresponding to the point targets and the surface roughness are well pointed out as for instance in the river and water-land transitions. Compared to the P image, we observe that some features are discarded mainly near the linear features (e.g., in the middle of the P-SAR image). Figure 9b shows the P-SAR composite image with a threshold $\tau_j = 0.15$. This choice allows pointing out only the point targets as boats in the river or houses in the village.

The ATWD has already been used for enhancing the spatial resolution of multispectral images by exploiting the P image [17]. All features extracted from the P image are incorporated into the multispectral images. In our approach, the ATWD is used as method for improving the SAR image. However, features to be incorporated are selected through a measure based on the importance value of the wavelet coefficient in order to avoid the disturbance of the information content.

4. CONCLUSION

The main objective of the paper was to present a fusion method for facilitating the interpretation of the SAR image by exploiting the high spatial resolution panchromatic image as a complementary data. Since some features are absent in the SAR image as lines and edges, the incorporation of the *P* wavelet coefficients implies a better discrimination of features contained into the SAR image. Experimental results show that the ATWD is preferable to the standard HPF method since it allows incorporating efficiently spatial features according an appropriate choice of the wavelet coefficients based on its importance value. This approach allows avoiding the disturbance of the information contained into the SAR image.

ACKNOWLEDGMENT

The author wishes to thank Professor A. Ozer and Dr. C. Barbier of the University of Liège and Centre Spatial de Liège respectively, Belgium, for providing many of the image samples used in this paper.

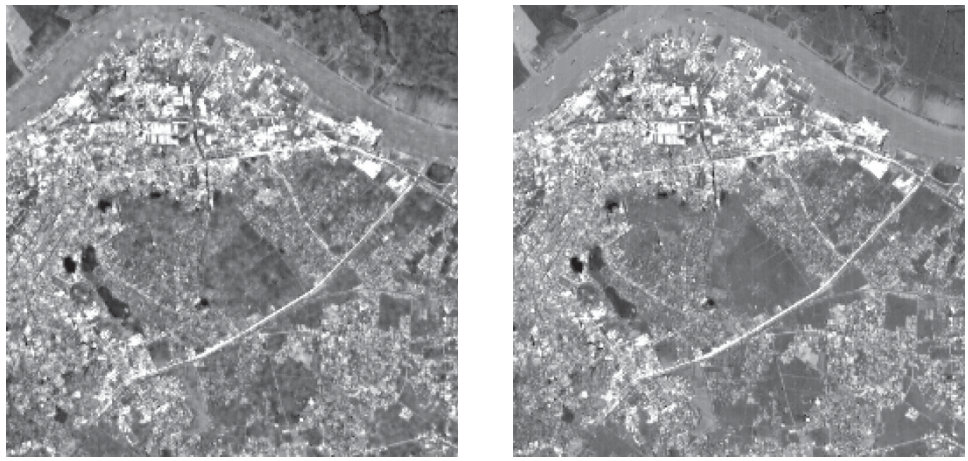

(a) (b)

Figure 9: P-SAR composite image obtained by using the ATWD with several thresholds: (a) ATWD: $N = 3$, $\tau_j = 0$; (b) ATWD: $N = 3$, $\tau_j = 0.15$.

REFERENCES

[1] J. F. Dallemand, J. Lichtenegger, R. K. Raney, and R. Schumann, *Radar Imagery: Theory and Interpretation*, Lectures Notes, FAO Remote Sensing Centre, Rome, Italy, 1993.

[2] C. Elachi, *Spaceborne Radar Remote Sensing: Applications and Techniques*, IEEE Press, New York, NY, USA, 1988.

[3] M. Rast, F. Jaskolla, and K. Arnason, "Comparative digital analysis of Seasat-SAR and LANDSAT-TM data for Iceland," *International Journal of Remote Sensing*, vol. 12, pp. 527–544, 1991.

[4] C. Pohl and J. L. van Genderen, "Review article Multisensor image fusion in remote sensing: concepts, methods and applications," *International Journal of Remote Sensing*, vol. 19, no. 5, pp. 823–854, 1998.

[5] S. G. Mallat, "A theory for multiresolution signal decomposition: the wavelet representation," *IEEE Trans. Pattern Anal. Machine Intell.*, vol. 11, no. 7, pp. 674–693, 1989.

[6] Y. Chibani and A. Houacine, "The joint use of the IHS transform and the redundant wavelet decomposition for fusing multispectral and panchromatic images," *International Journal of Remote Sensing*, vol. 23, no. 18, pp. 3821–3833, 2002.

[7] Y. Chibani and A. Houacine, "Redundant versus orthogonal wavelet decomposition for multisensor image fusion," *Pattern Recognition*, vol. 36, no. 4, pp. 879–887, 2003.

[8] M. Holschneider, R. Kronland-Martinet, J. Morlet, and Ph. Tchamitchian, "A real-time algorithm for signal analysis with the help of the wavelet transform," in *Wavelet: Time-Frequency Methods and Phase Space*, pp. 286–297, Springer-Verlag, Berlin, Germany, 1989.

[9] M. J. Shensa, "The discrete wavelet transform: wedding the à trous and Mallat algorithms," *IEEE Trans. Signal Processing*, vol. 40, no. 10, pp. 2464–2482, 1992.

[10] R. A. Schowengerdt, "Reconstruction of multispatial, multispectral image data using spatial frequency content," *Photogrammetric Engineering and Remote Sensing*, vol. 46, no. 10, pp. 1325–1334, 1980.

[11] M. Malfait and D. Roose, "Wavelet-based image denoising using a Markov random field a priori model," *IEEE Trans. Image Processing*, vol. 6, no. 4, pp. 549–565, 1997.

[12] L. J. Chipman, T. M. Orr, and L. N. Graham, "Wavelets and image fusion," in *Proc. IEEE International Conference on Image Processing (ICIP '95)*, vol. 3, pp. 248–251, Washington, DC, USA, October 1995.

[13] H. Li, B. S. Manjunath, and S. K. Mitra, "Multisensor image fusion using the wavelet transform," *Graphical Models and Image Processing*, vol. 57, no. 3, pp. 235–245, 1995.

[14] T. A. Wilson, S. K. Rogers, and L. R. Myers, "Perceptual-based hyperspectral image fusion using multiresolution analysis," *Optical Engineering*, vol. 34, no. 11, pp. 3145–3164, 1995.

[15] A. Bijaoui, J.-L. Starck, and F. Murtagh, "Restauration des images multi-échelles par l'algorithme à trous," *Traitement du signal*, vol. 11, pp. 229–243, 1994.

[16] A. Lopes, R. Touzi, and E. Nezry, "Adaptive speckle filters and scene heterogeneity," *IEEE Trans. Geosci. Remote Sensing*, vol. 28, no. 6, pp. 992–1000, 1990.

[17] J. Nùnez, X. Otazu, O. Fors, A. Prades, V. Palà, and R. Arbiol, "Multiresolution-based image fusion with additive wavelet decomposition," *IEEE Trans. Geosci. Remote Sensing*, vol. 37, no. 3, pp. 1204–1211, 1999.

Youcef Chibani was born in Algiers, Algeria. He received the Master and State Doctoral degree in electrical engineering from the University of Science and Technology Houari Boumediene, Algiers, Algeria. He is teaching and researching as an Assistant Professor since 2002. His research interests include the use of the wavelet decomposition, neural networks, and support vector machines in many applications as multisensor image fusion, change detection, and multimedia signal processing. He coauthored many papers published in international peer-reviewed journals and conferences.